Feng *et al. Cancer Nanotechnology* (2023) 14:33
https://doi.org/10.1186/s12645-023-00185-8

Cancer Nanotechnology

RESEARCH Open Access

Modulating tumour metabolism enhances gold nanoparticle radiosensitisation in HPV-negative head and neck cancer

Jie Feng[1], Varun Pathak[2], Niall M. Byrne[1], Tongchuan Wang[1], Cancan Yin[1], Reinhold J. Medina[2] and Jonathan A. Coulter[1*]

*Correspondence:
j.coulter@qub.ac.uk

[1] School of Pharmacy, Queens University Belfast, 97 Lisburn Road, Belfast BT9 7BL, UK
[2] Wellcome-Wolfson Institute for Experimental Medicine, School of Medicine, Dentistry and Biomedical Sciences, Queen's University Belfast, Belfast, Northern Ireland, UK

Abstract

Background: Radiotherapy is a major therapeutic modality for locally advanced head and neck cancer. However, the effectiveness of radiotherapy is hindered by resistance mechanisms, most notably hypoxia, leading to unfavourable treatment outcomes. In this study, we investigate the radiosensitising potential of AuNPs in combination with the complex III electron transport chain inhibitor, using models of head and neck cancer.

Results: AuNP intracellular accumulation occurred in a concentration-dependent manner and was not influenced by microenvironmental oxygen levels, with citrate capped 15 nm AuNPs readily internalised, accumulating primarily within the cytoplasmic compartment. Pre-treatment with atovaquone had a profound and rapid impact on oxygen consumption, promoting a glycolytic switch under both normoxic and hypoxic conditions, a finding underlined by the concurrent increase in extracellular acidification. AuNPs alone sensitised FaDu cells to radiation under atmospheric oxygen conditions, producing a sensitiser enhancement ratio (SER) of 1.37. In combination with atovaquone, maximum dose enhancements were achieved yielding a SER value of 1.43 and 2.1 under normoxic and hypoxic conditions, respectively. Studies to elucidate the underlying mechanism of radiosensitisation revealed S-phase accumulation and a significant increase in apoptosis. Additionally, combined treatment significantly increased yields of unrepaired DNA double strand breaks, indicating increased yields of DNA double strand break damage.

Conclusions: Taken together, we believe this to be the first work providing evidence that AuNP radiosensitisation can be enhanced via metabolic modulation. This study reveals the dual action of both physical and biological pathways of AuNPs radiosensitisation, resulting in superior radiotherapeutic effects.

Keywords: Metabolic radiosensitisation, Atovaquone, Gold nanoparticles, Head and neck cancer

Introduction

Head and neck squamous-cell carcinoma (HNSCC) is frequently an aggressive cancer with a high risk of recurrence. HNSCC is the 8th most common cancer in the UK, accounting for 3% of all new cancer cases and 2% of all cancer deaths (2016) (Shaw and Beasley 2016). Currently, surgery, radiotherapy and chemotherapy, in various combinations, are used in the treatment of HNSCC. The final treatment choice is dependent on disease locality, stage at diagnosis, HPV status, potential side effects, patient preference and overall health status (Brizel et al. 1998; Bonner et al. 2006; Vermorken and Specenier 2020; Cooper et al. 2004). For locally advanced HNSCC (LA-HNSCC), concomitant radio-chemotherapy remains the standard-of-care treatment, with HPV-positive tumours displaying greater radiosensitivity compared to HPV-negative tumours. This is reflected in the superior 3year survival data in response to radio-chemotherapy for HPV-negative [HPV (−)] (57.1%) versus HPV-positive (82.4%) (Göttgens et al. 2018; Mirghani et al. 2015). Despite the fact that concomitant radio-chemotherapy is proven to extend overall survival, yielding improved the quality of life, long-term disease-free survival is rarely achieved due to intrinsic tumour resistance (Perri et al. 2015). This highlights an important area of unmet clinical need to develop innovative strategies for the treatment of HPV(−) HNSCC.

Radiotherapy is a critical component in cancer management for more than 50% of cancer patients (Joiner and Kogel 2018; Delaney et al. 2005). In head and neck cancer, radiotherapy is widely utilised for treatment of primary disease and as an adjuvant with high local–regional control (Cooper et al. 2004). However, dose-limiting radiotoxicity represents a major challenge that limits the efficacy of the conventional radiotherapy (Bentzen 2006). One approach to overcome these obstacles is radiation dose enhancement, improving dose to the tumour while sparing surrounding normal tissue (Janic et al. 2021). This can be achieved through modulating tumour radiation response using radiosensitisers (Gong et al. 2021). Examples of radiosensitisers include oxygen mimics, cisplatin, hypoxia specific toxins, iodinated DNA targeting agents, inhibitors of DNA damage repair proteins and high atomic number materials such as gold and gadolinium (Gong et al. 2021; Wang et al. 2018; Chen et al. 2020).

Over the past decade, gold nanoparticles (AuNPs) have been widely explored as radiosensitisers due to their excellent physical and chemical properties (Her et al. 2017; Butterworth et al. 2012; Penninckx et al. 2020; Schuemann et al. 2020). AuNPs exploit the X-ray absorption properties of gold, where interactions with radiation destabilise atomic orbital electrons, resulting in a highly localised increase in radiation dose deposition, ultimately augmenting the effects of radiotherapy (Hainfeld et al. 2008). Radiosensitisation by AuNPs remains an active area of research in preclinical settings, with numerous studies demonstrating efficacy both in vitro and in vivo (Hainfeld et al. 2004; Cui et al. 2017; Jeremic et al. 2013). AuNPs are reported to complement the biological and chemical interaction of ionising radiation through the induction of ROS, cell cycle synchronisation, increased DNA damage yields, and via bystander effects (Rosa et al. 2017; Kempson 2021). However, the radiosensitising potential of AuNPs within the hypoxic microenvironment is often compromised, an effect attributed to compromised nanoparticle uptake, a reduction in reactive oxygen species and by the upregulation of various pro-survival hypoxia–inducible genes (Jain et al. 2014). These factors contribute to

the development of radiation resistance, leading to tumour relapse and treatment failure. Therefore, a potential strategy to further augment AuNP radiosensitisation is the combined treatment with hypoxia modifying drugs, sensitising this treatment resistant microenvironment.

Hypoxia is a common feature of most solid tumours occurring in approximately 80% of head and neck tumours (Bittner and Grosu 2013). The intrinsic radiation resistance of hypoxic cells represents a significant obstacle to the successful application of radiotherapy (Rockwell et al. 2009). Numerous clinical studies have proven tumour hypoxia as a potent negative prognostic factor in head and neck cancer, with low oxygen levels correlating with reduced treatment efficacy and decreased overall survival (Brizel et al. 1997; Linge et al. 2016; Eschmann et al. 2005). To date, most attempts to ameliorate the negative impact of hypoxia involved either increasing endogenous oxygen levels by perfusion of high concentrations of oxygen, or by targeting specific subpopulations of hypoxic tumour cells using hypoxia activated prodrugs (HAPs) (Curtis et al. 2016). While effective in the experimental setting, these approaches yielded only modest benefit in the clinical context (Spiegelberg et al. 2019). A recent study revealed that a Warburg phenotype in tumour cells, resulted in impaired mitochondrial respiration, enhancing radiosensitivity compared to genetically matched parental cells (Bol et al. 2015). This effect was related to a differential metabolic rate and aberrant oxygen consumption, suggesting that suppression of mitochondrial metabolism could potentially increase susceptibility to radiotherapy (Yasui et al. 2017). Such an approach represents a potential strategy for all hypoxic tumours, not solely restricted to tumours where oxidative phosphorylation activity is upregulated. Furthermore, in silico models also indicate that reduced oxygen consumption holds more potential than elevating blood flow or promoting oxygen delivery, with a 30% decrease in oxygen consumption retaining sufficient molecular oxygen to abolish severe radiobiological hypoxia (Spiegelberg et al. 2019). Conversely, an 11-fold increase in arterial partial pressure of oxygen (pO_2) is required to achieve a comparable level of oxygenation (Grimes et al. 2014). Currently, several pharmacological drugs that inhibit cellular oxygen consumption have been investigated for their potential to increase tumour oxygenation and thereby enhance radiosensitivity. Metformin, papaverine, arsenic trioxide and atovaquone are all known to influence tumour cell metabolism by modifying oxygen consumption (Benej et. al 2018; Diepart et al. 2012)

Atovaquone, an FDA approved drug, is a complex III inhibitor, originally used for the prevention and treatment of pneumocystis pneumonia and toxoplasmosis in HIV patients (Fry and Pudney 1992; Araujo et al. 1991). Atovaquone has recently been repurposed as hypoxia modifier, where atovaquone treatment induced an 80% reduction in tumour hypoxia in a range of tumour cell models through targeted inhibition of mitochondrial complex III activity. Importantly, this effect contributed to a significant tumour growth delay when combined with radiotherapy (Ashton et al. 2016). In addition, atovaquone also showed efficacy in the treatment of ovarian and breast cancer stem cell populations, a rare sub-population of cells linked with development of radioresistance and tumour relapse (Fiorillo et al. 2016; Guo et al. 2021). While current work with atovaquone as hypoxia modifier is still at early stage, the ability of atovaquone to alleviate tumour hypoxia appears promising. A recent clinical trial (NCT02628080) demonstrated that atovaquone reduced tumour hypoxia by up to 55% in non-small cell lung

cancer patients (Skwarski et al. 2021). Encouragingly, the authors also reported that the most intensely hypoxic tumour voxels, i.e. the most radiologically resistant regions, were subjected to the most pronounced reduction in hypoxia, providing important insights into the action of atovaquone as a novel radiosensitiser (Bourigault et al. 2021).

In this study, we investigate the effect of targeting multiple pathways of radiosensitisation as an approach to enhance the radiotherapeutic potential in HPV(−) HNSCC. We hypothesise that the combination of AuNPs, which endow physical dose enhancement, with atovaquone as metabolic modulator should result in a greater degree of radiosensitisation compared to either agent alone. To test our hypothesis, we evaluated the radiosensitising effects of AuNPs in combination with atovaquone. The effect on nanoparticle uptake, apoptosis, and radiation-induced DNA damage will be evaluated to elucidate the underlying mechanisms of radiosensitisation conferred by the combined treatment.

Materials and methods

Chemicals

Atovaquone was purchased from Sigma-Aldrich [UK) and was dissolved in 100% DMSO to make a 30 μM stock solution. All drug stock solutions were stored at − 20 °C for future experimental use.

Cell lines and reagents

CAL27 cells were obtained from the American Type Culture Collection [ATCC), and FaDu and CAL33 cells obtained from DSMZ [Brauschweig, Germany). CAL27 cells were grown in Dulbecco's modified Eagle's medium [DMEM, Sigma-Aldrich) supplemented with 2% HEPES (1 M, PAA laboratories), 1% sodium pyruvate (100 mM, Sigma), 1% non-essential amino acids (100x, Sigma), 10% foetal bovine serum (FBS, Gibco) and 1% L-glutamine (200 mM, Sigma-Aldrich). FaDu and CAL33 cells were maintained in Eagle's minimum essential medium (EMEM, ATCC) with 10% FBS. All routine culturing was carried out at 37 °C and 5% CO_2/95% air. Short tandem repeat profiling and mycoplasma testing (Lonza) were conducted routinely for these cell lines.

Synthesis of AuNPs

AuNPs were prepared according to the classical Turkevich method (Turkevich et al. 1951). Briefly, 400 mL of 0.01% chloroauric acid ($HAuCl_4.4H_2O$) solution was heated and refluxed in a round-bottom flask. Next, 9.6 mL of 1% sodium citrate solution was added to the boiling solution to obtain the AuNPs. The reduction of gold chloride by sodium citrate was completed after 5 min. The solution was further boiled for 30 min, then left stirring overnight at room temperature. Finally, the resultant colloidal solution was centrifuged at 12,000 rcf for 90 min and washed with distilled water.

Quantitative evaluation of AuNP uptake in cell monolayers

Cells were seeded in 6-well plates at a density of 4×10^5 cells/well and incubated overnight. Growth media was then replaced with fresh media containing different concentrations of AuNPs (0, 5, 10, 50, 100 μg/mL of gold). Following a 24 h treatment period, media containing excess extracellular AuNPs was removed, cells were then washed three times with PBS and harvested using 1×trypsin. Cells were counted and centrifuged at

500 g for 5 min, supernatant removed, and the cell pellet digested using 1 mL aqua regia. Samples were then made to a total volume of 5 ml using Milli-Q water. For hypoxic uptake experiments, cells were seeded into 6-well plates and allowed to adhere under atmospheric oxygen conditions overnight. The following day cells were transferred to a hypoxic workstation station (In Vivo2 400, Baker Ruskinn, UK) for 4 h, then treated with AuNPs at differing concentrations for a further 24 h. The concentration of internalised gold was measured by inductively coupled plasma atomic emission spectroscopy (ICP-AES) and reported as concentration of gold (pg) per cell.

Qualitative evaluation of AuNPs internalisation using hyperspectral microscopy

Enhanced darkfield/hyperspectral Cytoviva microscopy was employed for the optical observation and spectral confirmation of nanoparticle internalisation. Within these optical images AuNPs appear bright due to their high scattering cross section. To confirm the presence of AuNPs, the plasmonic resonance properties of gold was detected by spectra angle mapping (SAM) using the Cytoviva hyperspectral imaging system. This system confirms internalisation and intracellular location by comparing the unknown spectra in the acquired hyperspectral image against a user defined spectral library, i.e. that of AuNPs. Briefly, 4×10^4 cells were seeded into a 4-well glass chamber slide (Corning, USA). After 48 h, cells were treated with media containing AuNPs for 24 h, washed three times with PBS and fixed using 10% formalin. Under hypoxic conditions cells were transferred to a hypoxia chamber (0.5% O_2) and incubated for 4 h before a 24 h AuNPs treatment, then washed, fixed and imaged.

Seahorse X-Fe 96 metabolic flux analysis

The bioenergetic function of HPV(−) HNSCC cells treated with atovaquone was determined using Seahorse Extracellular Flux analyser (Seahorse Bioscience, MA, USA). In brief, 2×10^4 cells per well were seeded into seahorse X-Fe 96-well culture plates and incubated overnight to allow attachment. Cells were then washed with pre-warmed XF assay DMEM medium for OCR (oxygen consumption rate) measurement. XF assay media was supplemented with 10 mM glucose, 1 mM sodium pyruvate, 2 mM L-glutamine and adjusted to pH = 7.4. Cells were maintained in 180 µL/well of XF assay media, in a non-CO_2 incubator for 1 h. During the incubation period, 20 µL of (150, 300 µM) diluted in seahorse XF medium was loaded into the injection ports in the XFe-96 senor cartridge. After establishing a baseline OCR and extracellular acidification rate (EACR), atovaquone was administered thorough an automated pneumatic injection port. Subsequent changes in OCR and ECAR were monitored over a 3 h period. The resulting effects on OCR and ECAR are shown as percentages of the baseline for respective treatments. For hypoxia OCR and ECAR measurements, all manipulations including seahorse analyses, were carried out within a hypoxic chamber at 1% O_2.

Clonogenic assays

Clonogenic assays were performed according to our previously published reports [50]. In brief, 4×10^5 cells were plated in a 35 mm^2 dish and allowed to adhere for 24 h. Cells were then treated with 100 µg AuNPs and/or atovaquone for 24 h, then irradiated with a single dose of 2, 4 or 6 Gy. For hypoxic studies, cells were seeded and allowed to attach

at 37 °C, 5% CO_2/95% air overnight before being transferred to hypoxic station with 0.5% O_2, 5% CO_2, 95% nitrogen for 4 h allowing equilibrium. Cells were then treated with either AuNPs (100 μg), atovaquone or combination of AuNPs and atovaquone for 24 h, prior to radiation treatment at 0.5% O_2, 5% CO_2. Following radiation treatments, cells were washed twice in PBS, trypsinised, counted, and reseeded in 6-well plates before incubating for a further 9–14 days under atmospheric oxygen conditions, allowing colony formation. Colonies were then fixed and stained using 70% methanol and 0.4% crystal violet. Colonies with more than 50 cells were counted to determine plating efficiency (PE), where PE is defined as the number of colonies formed divided by the number of cells seeded. Surviving fractions (SF) were then calculated relative to non-irradiated controls and fitted to the linear quadratic (LQ) equation (Eq. 1).

$$\text{Linear quadratic: } S = \exp(-\alpha D - \beta D^2) \tag{1}$$

LQ fits were calculated using least-square regression in prism 9.0 (GraphPad Software, CA, USA). The area under the curve (AUC), which represents the mean inactivation dose (MID), was obtained and the sensitiser enhancement ratio (SER) calculated by dividing the MID of non-exposed cells with AuNPs or atovaquone treated cells. α and β components have been derived from the linear quadratic fit, representing the ratio of either direct (α) and indirect (β) cell damage.

Cell cycle analysis

Cells were seeded in 6-well plates at a density of 8×10^5 cells/well, then incubated overnight. The next day growth medium was replaced with fresh medium containing atovaquone, AuNPs (100 μg/mL) or the combination of AuNPs and atovaquone for a further 24 h. Cells were then irradiated using a single 4 Gy dose and returned to the incubator for a further 24 h before fixing. Monodisperse cells were washed in PBS and resuspended in 0.5 mL of propidium iodide (containing 50 μg/mL PI and 10 μg/mL RNase) for 30 min at 4 °C. Analysis was performed using a BD FACSCalibur flow cytometer. Cell cycle analysis was performed in triplicate with data from a minimum of 10,000 cells per sample collected. Cell cycle data analysis was performed using FlowJO software.

Cell apoptosis assay

Quantitative analysis of apoptosis was performed by flow cytometry using an Annexin-FITC-propidium iodide (PI) apoptosis detection kit (BD Biosciences, USA). In short, cells were incubated at a density of 2×10^5 cells/well in 6-well plates, and allowed to attach for 24 h. Cells were then exposed to either hypoxic (0.5% O_2) or atmospheric oxygen (21% O_2) conditions and treated with medium containing atovaquone, AuNPs (100 μg/mL) or the combination of AuNPs and atovaquone for a further 24 h prior to radiation treatment. As with cell cycle analysis, apoptosis assays were performed 24 h post-radiation treatment. The subsequent procedure was performed in accordance with the manufacturer protocol. Briefly, cells were washed twice with cold PBS, then suspended in 195 μL binding buffer at a cell density of 5×10^5 cells/mL. After a 10-min incubation with 5 μL of Annexin V-FITC, cells were resuspended in 190 μL binding buffer including 10 μL of PI. After incubation for 15 min at room temperature in the

dark, samples were analysed by flow cytometry (BD FACSCalibur). Data analysis was performed using BD FACSuiteTM software.

DNA damage analysis by immunofluorescence assay

Immunofluorescence assays were performed as described previously [50]. Cells were plated in 4-well chamber slides at a density of 4×10^4 cells per well and left to adhere for 48 h. Cells were then treated with atovaquone (30 μM), and/or AuNPs (100 μg/mL) for a further 24 h before IR treatment using a single fraction dose of 2 Gy (Faxtrion CP-160 Arizona USA). After IR treatment cells were returned to the incubator for either 2 h or 24 h, allowing partial DNA damage repair. Cells were then washed with PBS and fixed with 4% formaldehyde, permeabilised using 0.1% PBS-Tween 20, and blocked with 1% BSA for 1 h. Cells were then incubated with primary 53BP1 antibody (1:1000 dilution in 1% BSA). As indirect immunofluorescence was used, cells were then washed three times with PBS for 5 min and incubated with Alexa flour 488 secondary antibody (1:1000 dilution in 1% BSA) at room temperature in the dark. Finally, cells were washed three times with PBS before drying and mounting with DAPI (Abcam, UK). With respect to quantifying residual DNA damage, for each replicate 53BP1 foci from 50 cells per treatment were scored.

Statistical analysis

All statistical analysis were performed using GraphPad Prism 9 software. Scientific data were expressed as mean ± SEM. For clonogenic assays, two-way analysis of variance (ANOVA) was performed with Turkey multiple tests to determine statistical differences between treatment groups. For all other experiments, comparisons between multiple groups were performed using one-way analysis of variance with Turkey multiple tests. Data are shown as statistically significant when p-value of equal to or less than 0.05 were recorded.

Results

Cell uptake and location of AuNPs

Intracellular concentration and localisation of AuNPs are two important factors that markedly influence tumour cell sensitivity to radiation treatment. AuNP internalisation was assessed both quantitatively and qualitatively using ICP-AES and hyperspectral imaging. Quantitative assessment of AuNPs uptake demonstrated a clear positive correlation with treatment concentration under both hypoxic and normoxic conditions, across all three cell lines tested (Fig. 1). More specifically, AuNPs internalisation proved to be significantly ($p < 0.01$) increased at 100 μg/ml AuNP treatment over 10 μg/ml or below, an effect consistent to all cell models. Intracellular Au concentrations of 64 ± 24 pg/cell, 68 ± 17 pg/cell and 75 ± 23 pg/cell, were achieved in FaDu, CAL27 and CAL33 cells (Fig. 1a–c), respectively. Hypoxic stress had no obvious impact on AuNP uptake, with total intracellular Au levels slightly increased in all three cell lines over cells maintained under environmental oxygen conditions (FaDu—86 ± 19 pg/cell, CAL27—80 ± 2 pg/cell, and CAL33—97 ± 19 pg/cell, respectively).

Intracellular AuNP uptake and localisation was also visualised using hyperspectral imaging. Darkfield imaging indicates significant nanoparticle internalisation by the

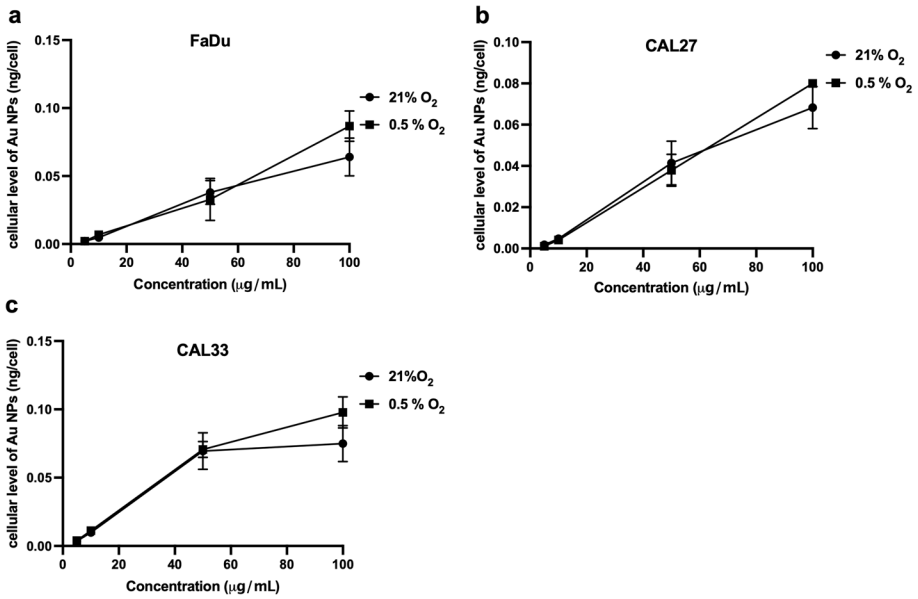

Fig. 1 Cell uptake of AuNPs in FaDu (**a**), CAL27 (**b**) and CAL33 (**c**) cells under atmospheric (21% O_2) or hypoxic (0.5% O_2) conditions. One-way ANOVA followed by Turkey's multiple tests was used to compare within different concentrations, * $p < 0.05$, ** $p < 0.01$, *** $p < 0.001$, **** $p < 0.0001$. Data were obtained from three independent experiments performed in triplicate ± SEM

presence of multiple bright focal regions following 24 h nanoparticle treatment. Using integrated pixel-by-pixel hyperspectral filtering against the untreated control, false positive signals are eliminated, producing a spectral angle map (SAM) confirming AuNP intracellular locality. At this resolution, predominant AuNP intracellular accumulation appears to co-localise within a perinuclear region (Fig. 2), mostly likely within endoplasmic reticulum due to endosomal vesicle trafficking. As with quantitative uptake studies, similar observations were also observed under hypoxic conditions (Additional file 1: Figure S1).

Effect of atovaquone on bioenergetic function in HPV(−) HNSCC cells

Atovaquone mediated inhibition of respiratory capacity would be expected to significantly alter the tumour cell metabolic profile, enabling adaption to treatment related stress. To test this, we measured the bioenergetic function of FaDu, CAL27 and CAL33 cells in response to atovaquone using the Seahorse Bioscience XF96 analyser, with experiments conducted under 21% O_2 and 1% O_2. Cells were analysed for both oxygen consumption rate (OCR) and extracellular acidification (ECAR—a surrogate readout of lactic acid efflux). Atovaquone greatly reduced OCR in all cells under normoxic (Fig. 3) and hypoxic (Additional file 1: Figure S2) conditions, with hypoxia notably decreasing OCR by roughly 50% in the control group. More specifically, a marked OCR decrease was observed in FaDu cells using atovaquone at both 15 and 30 μM under normoxia (Fig. 3a), reducing OCR by 76% over untreated controls. A similar degree of OCR suppression was also observed in CAL27 and CAL33 cells (Fig. 3b–c), reducing OCR by approximately 80%. Encouragingly, if adopting this strategy to help alleviate hypoxia induced radioresistance, a similar pattern was also observed under hypoxic conditions following atovaquone treatment (Additional file 1: Figure S2a–c), maximally suppressing

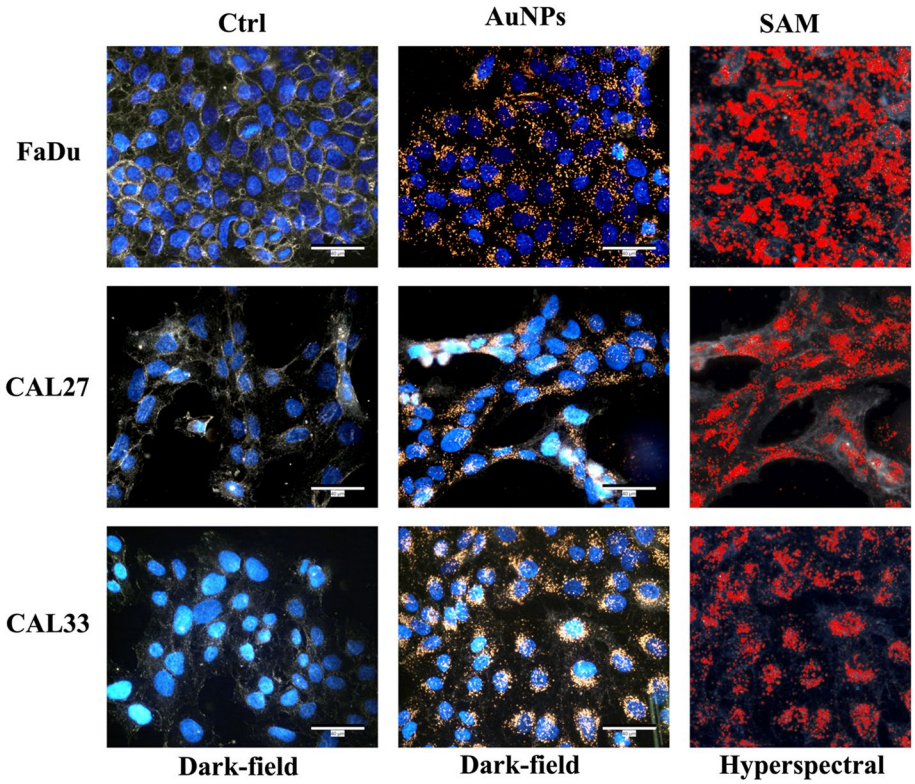

Fig. 2 Intracellular uptake and localisation of AuNPs within FaDu, CAL27 and CAL33 cells under atmospheric oxygen conditions using Cytoviva darkfield/hyperspectral imaging. Cells were treated with AuNPs for 24 h, fixed and mounted with DAPI before imaging. Representative images include enhanced dark field and the corresponding hyperspectral images, overlaid with a spectral angle map (SAM) representing AuNPs in red

OCR by 87.6%. This meant that atovaquone treatment effectively doubled the reduction in OCR relative to hypoxia alone, proving effective even under hypoxic conditions.

Parallel to the changes in the mitochondrial respiration, we also observed that atovaquone stimulated a concomitant increase in ECAR, indicating a switch to glycolytic metabolism, likely compensating for ATP depletion due to respiratory stress. Atovaquone elevated the extracellular acidification by 2.3-fold in FaDu cells over untreated controls (Fig. 3d). This effect was even more pronounced in CAL27 and CAL33 cells, resulting in an approximate fourfold increase in ECAR, irrespective of drug concentration (Fig. 3e–f). Under hypoxic conditions, similar effects were also observed in all three cell lines tested (Additional file 1: Figure S2), with the greatest effect seen in CAL33 cells, yielding a 2.5-fold ECAR increase (Additional file 1: Figure S2f).

Modified radiation sensitivity using AuNPs and atovaquone

AuNPs are proven radiosensitisers, nevertheless the magnitude of effect is often compromised under hypoxic conditions (Jain et al. 2014). Herein we investigated whether AuNPs, which act as both physical and chemical radiation dose modifiers, combined with atovaquone, increase the radiosensitivity of HNSCC cells compared to either agent alone. In the absence of radiation, AuNP, atovaquone or the combined treatment showed no significant toxicity as evidenced by the minimal changes in SF_0

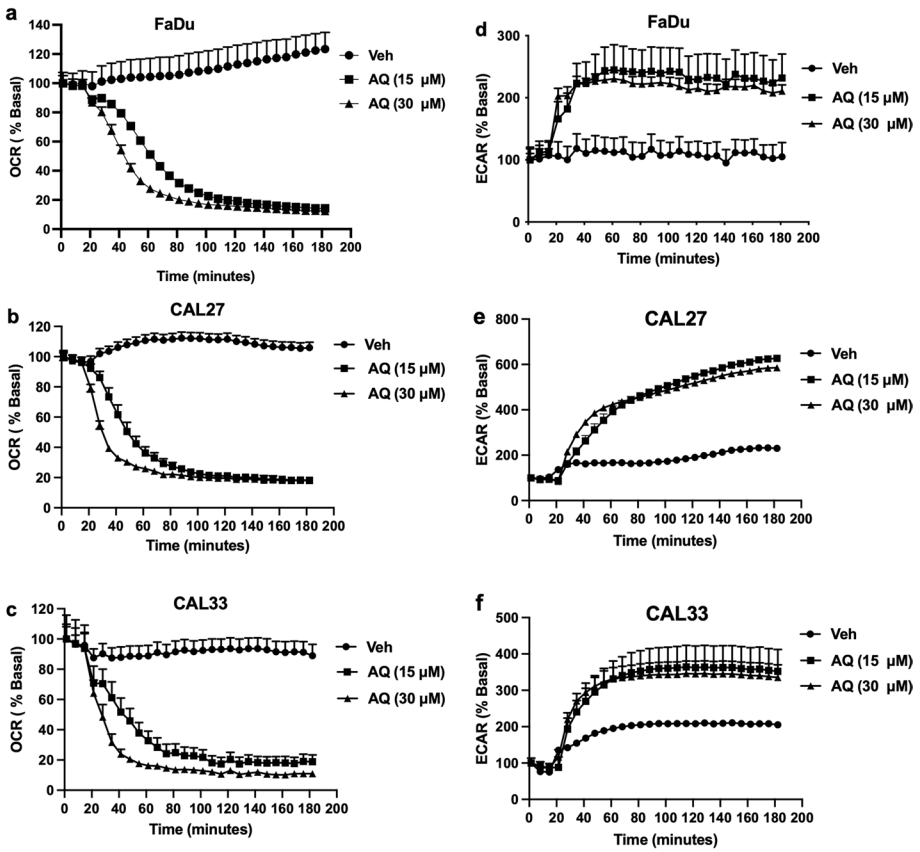

Fig. 3 Bioenergetic profile of HNSCC cells treated with atovaquone (AQ) under 21% O_2. Changes in oxygen consumption rate (OCR) and extracellular acidification rate (ECAR) were monitored at 37 °C for 3 h. The resulting effect of atovaquone on OCR and ECAR is shown as a percentage of the baseline measurement after each treatment. Data shown are the means ± SEM ($n = 5$ per treatment group)

values under both normoxia and hypoxia (Additional file 1: Figure S3). Radiation survival curves for all treatment groups along with dose enhancement factors (DEF) at 2 Gy and 4 Gy are provided in Fig. 4 and in the supporting information (Additional file 1: Table S1). AuNPs alone significantly sensitised all three cell lines to radiation treatment under atmospheric oxygen conditions, producing mean sensitiser enhancement ratios (SER) of 1.37, 1.33 and 1.37 for FaDu ($p = 0.0122$), CAL27 ($p < 0.0001$) and CAL33 cells ($p = 0.0002$), respectively. Atovaquone alone significantly increased radiation sensitivity in FaDu cells ($p = 0.0463$), generating a SER of 1.43 (Fig. 4a). However, drug alone failed to modulate radiation response in CAL27 and CAL33 cells (Fig. 4b–c). Using an equivalent concentration of atovaquone combined with AuNPs markedly augmented radiation sensitivity ($p = 0.0002$), yielding an SER of 1.72 in FaDu, equating to an additional 35% increase in radiation sensitivity over single agent treatment with AuNPs alone. Conversely, the combined treatment of AuNP and atovaquone failed to significantly enhance radiation sensitivity over AuNPs alone in CAL27 and CAL33 cells (Fig. 4b–c), implying that in these cells radiation dose enhancement is predominately mediated by AuNPs. Interestingly, in an era where hypofractionation and stereotactic radiotherapy are increasingly pushing the clinical limits of dose fractionation, the radiosensitising potential of combining these two

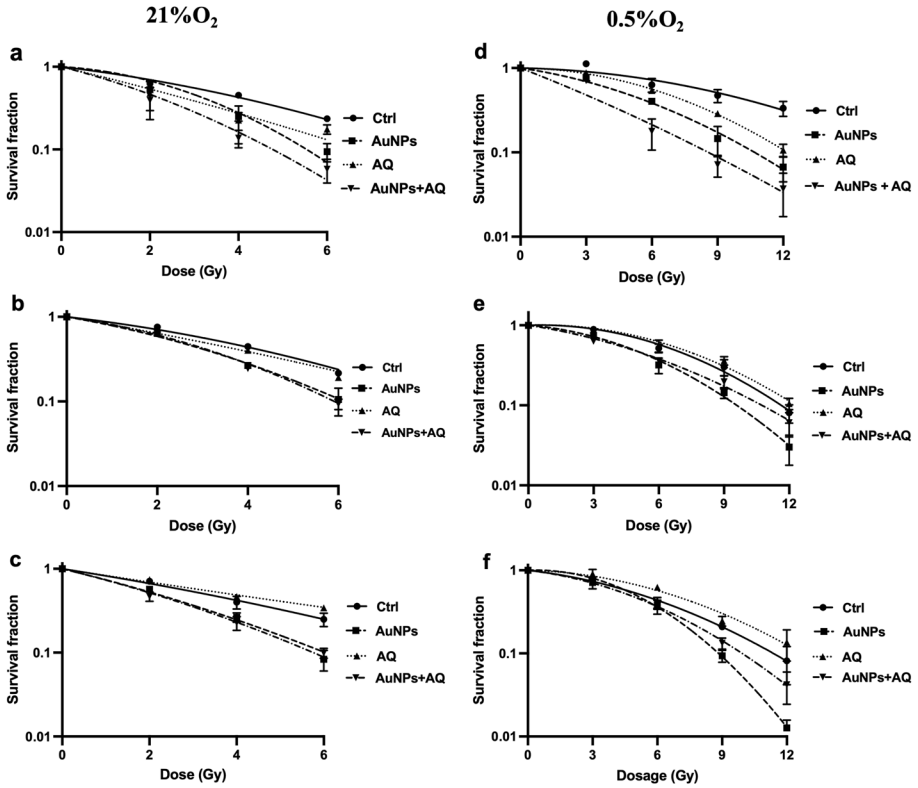

Fig. 4 Clonogenic radiation survival curves for FaDu (**a** and **d**), CAL27 (**b** and **e**) and CAL33 (**c** and **f**) cells treated with either AuNPs (100 μg), atovaquone (AQ, 30 μM) or the combination of both under normoxic (**a**, **b** and **c**) and hypoxic (**d**, **e** and **f**) conditions. Two-way ANOVA with Turkey multiple comparison test was used to compare within different treatments. Significant differences are represented by $*p < 0.05$, $**p < 0.01$, $***p < 0.001$. Data were obtained from three independent experiments performed in triplicate ± SEM

agents appear to increase with dose, evidenced by an increased DEF of 2.64 at 4 Gy in FaDu cells (Additional file 1: Table S1).

The radiosensitising effect for the combined use of AuNPs and atovaquone was also investigated under hypoxic conditions. Unsurprisingly, hypoxia severely impaired radiation sensitivity, with an approximate oxygen enhancement ratio (OER) of 2, indicating that hypoxia was maintained during radiation treatment, and that hypoxia induced radioresistance was observed. Encouragingly, under hypoxic conditions, the combination of AuNP and atovaquone again resulted in a significant ($p = 0.049$) increase in FaDu radiosensitivity (SER 2.1) over treatment with AuNP alone (Fig. 4f). As observed under normoxia, atovaquone alone failed to significantly modulate the response to radiotherapy in CAL27 and CAL33 cells, an effect recapitulated in the combined treatment group.

Effect of AuNP and atovaquone treatment on cell cycle distribution

To explore further the potential mechanism underpinning AuNP/atovaquone radiosensitisation, the effect of treatment on cell cycle distribution was evaluated. Combinations of AuNP and atovaquone induced a significant ($p < 0.05$) increase in the ratio of S-phase FaDu cells under 21% O_2 (Fig. 5a, Additional file 1: Fig S4a). Furthermore, combined with a 4 Gy radiation dose, atovaquone significantly ($p = 0.014$)

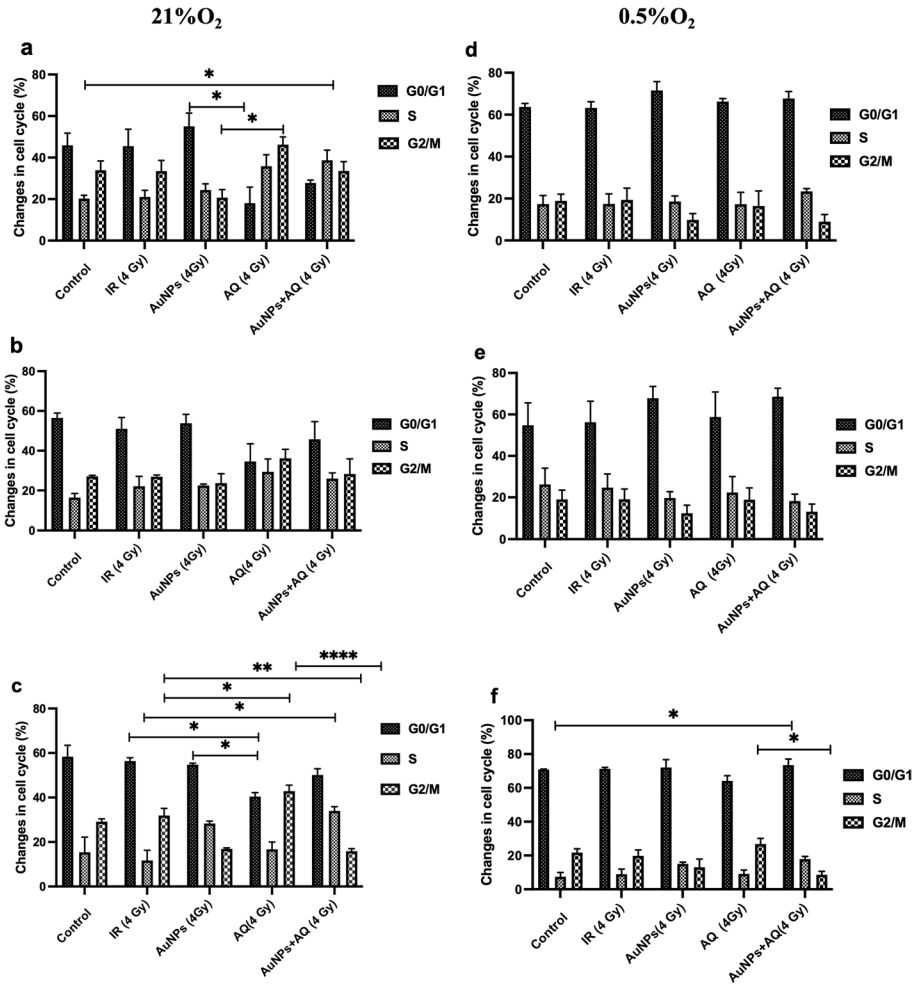

Fig. 5 Cell cycle distribution of HNSCC cells 24 h after treatment with AuNPs (100 µg) and/or atovaquone (AQ 30 µM), alone or in combination with radiation (4 Gy) under both 21% O_2 and hypoxic conditions (0.5% O_2). One-way ANOVA followed by Turkey's multiple tests was used to compare within different treatments, significant differences are represented by $^{*}p < 0.05$, $^{**}p < 0.01$, $^{***}p < 0.001$, $^{****}p < 0.0001$. Data were obtained from three independent experiments performed in triplicate ± SEM

decreased the G_0/G_1 population compared to AuNPs + 4 Gy treated cells, from 55 to 18% ($p = 0.0143$). This response drove a concomitant increase in the proportion of G_2/M cells, doubling from 20.7% to 40.6% ($p = 0.0141$), Despite that no significant difference in clonogenic cell survival was observed in CAL33 cells, similar significant ($p = 0.0216$) drug/nanoparticle induced alterations in cell cycle distribution were observed, with a > 10% increase in G_2/M accumulation following atovaquone and radiation (Fig. 5c and Additional file 1: Fig S4a), an effect that was surprisingly impaired (42.9% to 15.9% ($p < 0.001$)) when AuNPs were added to the treatment combination. No statistically significant cell cycle alterations were observed in CAL27 cells irrespective of treatment (Fig. 5b and Additional file 1: Fig S4a). In a similar manner, under hypoxia, the various combinations of atovaquone/AuNP treatment had minimal impact on cell cycle distribution (Fig. 5d–e, and Additional file 1: Fig

S4b), except that we again observed a significant decrease in the G_2/M population of CAL33 cells following the combination treatment (Fig. 5f) ($p = 0.0126$).

Effects of AuNPs and atovaquone inhibitor treatment in apoptosis induction

Apoptosis significantly contributes to radiation-induced cell death (Rupnow and Knox 1999; Dewey et al. 1995; Verheij and Bartelink 2000). In the current study, the apoptotic response of HNSCC cells in response to atovaquone, AuNPs or the combination with and without radiation was evaluated using Annexin-FITC/PI staining (Fig. 6 and Additional file 1: Fig S5). Unsurprisingly, the combined treatment with radiation induced the highest proportion of apoptotic cells in all cells tested, proving statistically significant in FaDu (27%, $p < 0.01$—Fig. 6a) and CAL27 cells (25%, $p = 0.012$—Fig. 6b) compared to either AuNP or atovaquone as a monotherapy combined with radiation. In CAL33 cells the magnitude of response was similar, although not significant, with the observed increase in apoptosis predominantly driven by atovaquone (Fig. 6c). Interestingly, under

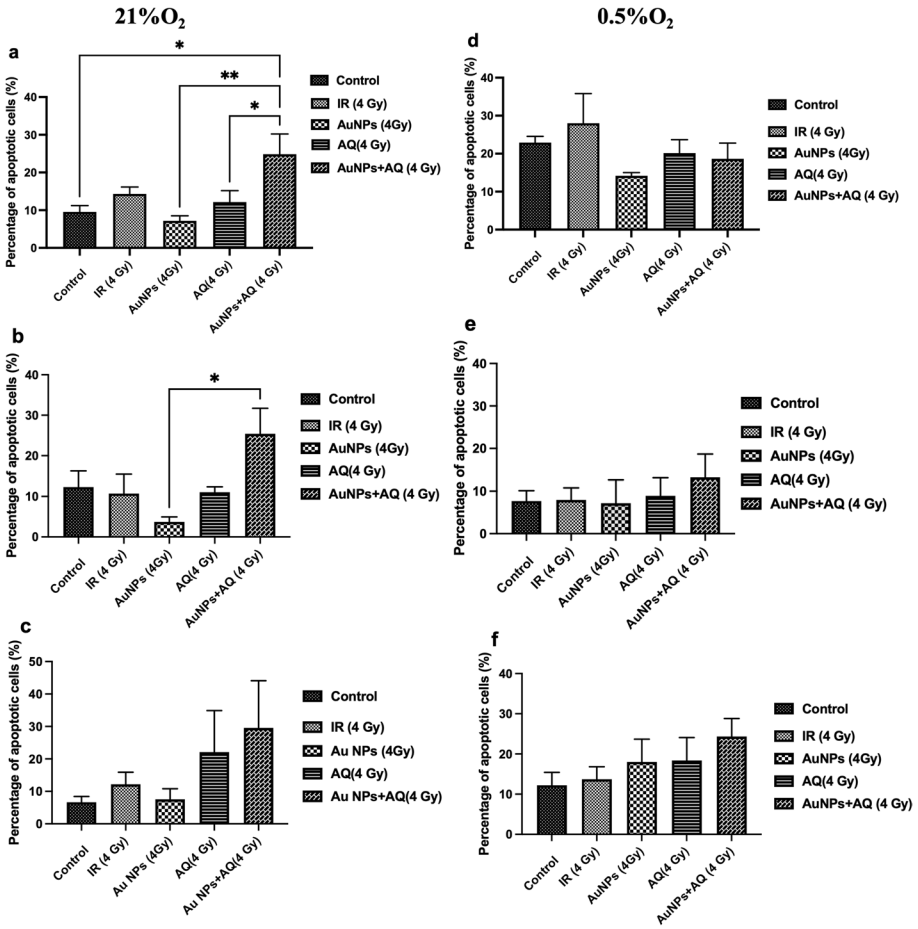

Fig. 6 Annexin V/PI staining for apoptosis in FaDu (**a**, **d**), CAL27 (**b**, **c**) and CAL33 (**e**, **f**) cells treated with AuNPs (100 µg), atovaquone (AQ 30 µM) or radiation (4 Gy) or the combination. Cells were maintained under atmospheric oxygen conditions (21% O_2—panels **a**, **b** and **c**) or hypoxia (0.5% O_2—panels **d**, **e** and **f**). Data presented are from at least three independent replicates performed in triplicate ± SEM. One-way ANOVA followed by Tukey's multiple comparisons test was used to compare within different treatments, significant differences are represented by $*p < 0.05$, $**p < 0.01$, respectively

hypoxia there was a trend towards increased basal apoptosis, likely triggered by hypoxia induced stress, with the overall combination effect of atovaquone and AuNP strongly attenuated (Fig. 6d–f) across all three cell lines.

Effects of AuNPs and atovaquone treatment on the induction of DNA DSBs

As DNA damage is the primary mechanism by which radiation triggers cell death, we next aimed to investigate if the combined effect of atovaquone and AuNP with radiation treatment increased DNA damage yields or interfered with DNA damage repair. 53BP1 foci were scored and used as a surrogate marker of DNA double strand breaks 2 h and 24 h post-radiation treatment. Figure 7a is representative images of FaDu 53BP1 foci. Radiation combined with either AuNP or atovaquone appeared to increase

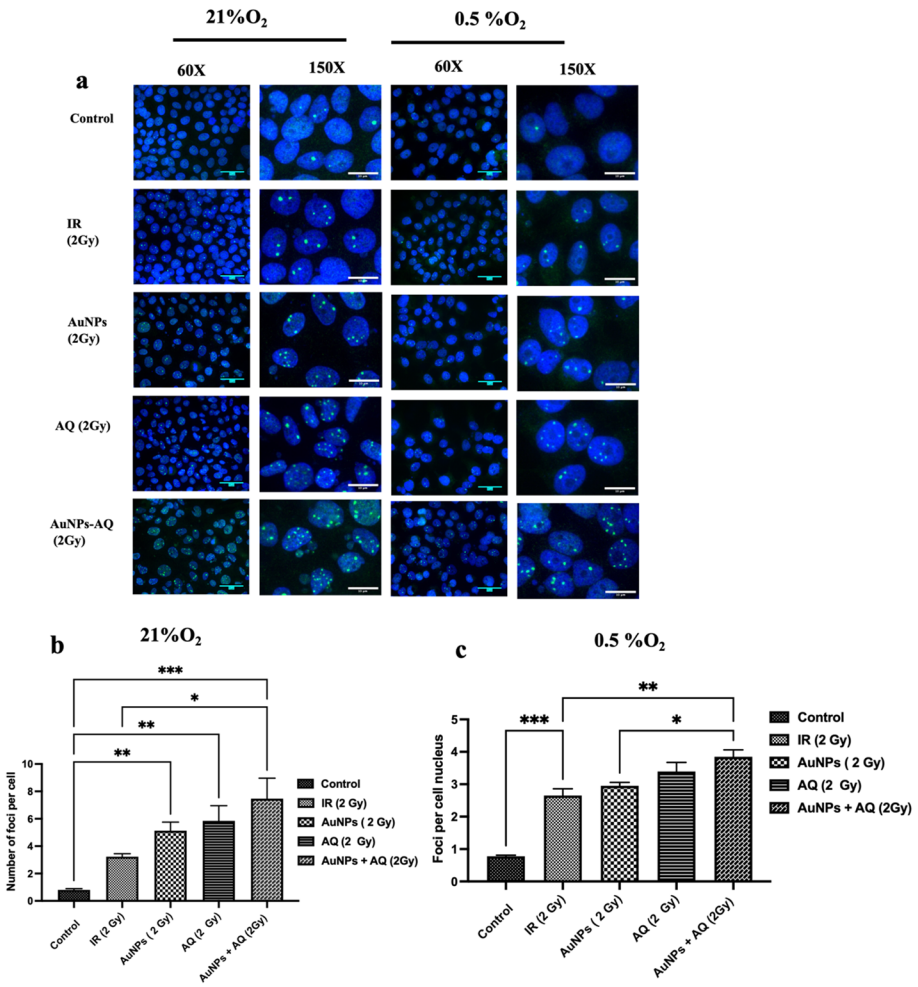

Fig. 7 (**a**) Representative immunofluorescence images of 53BP1 foci in FaDu cells 24 h post-radiation (2 Gy) under 21% O_2 and 0.5% O_2. Cells were treated with either AuNPs (100 µg), atovaquone (AQ 30 µM) or the combination. Panels **b** and **c** represent the mean 53BP1 foci 24 h post-radiation (0 or 2 Gy) in FaDu cells after treatment with AuNPs, atovaquone or the combination under atmospheric oxygen levels (**b**) and hypoxia (**c**). Data presented are from at least three independent replicates performed in triplicate ± SEM. One-way ANOVA followed by Turkey's multiple comparison test was used to compared within different treatment. * represents significant difference at $p < 0.05$, ** at $p < 0.01$, *** at $p < 0.001$

residual 53BP1 foci compared to 2 Gy alone, an effect that was augmented using combined AuNP/atovaquone, significantly ($p = 0.0124$) increasing residual DNA damage yields by 31% over radiation alone. Similar effects were also seen in CAL33 cells (Additional file 1: Figure S6), where the combination significantly ($p = 0.0338$) attenuated DNA damage over AuNPs alone, increasing unresolved DNA damage yields by 60%. This response was not observed in CAL27 cells (Additional file 1: Figure S7).

Hypothesising that reduced oxygen consumption would increase intracellular oxygen levels, therefore leading to further DNA damage, we next assessed the impact of the combined treatment on radiation-induced DNA damage under hypoxia at both 2 h and 24 h post-radiation. Additional file 1: Figure S8 shows representative and quantified data of 53BP1 foci in FaDu, CAL27 and CAL33 cells. The radiation treatment induced a significant increase in DNA damage, producing 15.6 ± 1.7, 12.0 ± 2.8 and 13.6 ± 3.9 for FaDu, CAL27 and CAL33 cells, respectively. Interestingly, the combined treatment with radiation and atovaquone further enhanced DNA damage yields over radiation alone, increasing double strand break formation by 47%. Figure 7 a&c are representative images and quantified data of 53BP1 foci in FaDu cells under 0.5% O_2, only this time 24 h post-irradiation, allowing time for DNA damage repair. Surprisingly, the mean residual DNA damage yields were elevated in the combination treatment, again by exactly 47%, indicating that the combination treatment increases DNA damage rather than interfering with DNA damage repair. In CAL27 and CAL33 cells, the combination of atovaquone and AuNPs plus radiation only slightly increased DNA DSB yields (Additional file 1: Figures S6, S7), failing to prove statistically significant.

Discussion

In the current study, AuNPs have been explored as an experimental radiosensitiser to enhance the biological effectiveness of conventional photon therapy due to their desirable physical and chemical properties (Cui et al. 2017; Choi et al. 2020) Various existing in vitro and in vivo studies have demonstrated the potential of AuNPs as effective radiosensitisers, capable of achieving dose enhancements comparable to those of approved radiosensitisers in routine clinical practice (López-Valverde et al. 2022; Khoo et al. 2017) However, clinical translation of AuNPs has been slow, attributed to several reasons including less well understood PK/PD properties over conventional small molecules, poor target cell internalisation and inconsistent impacts on redox activity, rendering these experimental agents less effective under hypoxic conditions(Jain et al. 2014; Cui et al. 2014). To overcome this challenge, we present a relatively unexplored strategy for increasing the radiosensitisation of AuNPs through the combined use of AuNPs with atovaquone, a metabolic modulator which could lead to increased tumour radiosensitivity through improved oxygenation. This approach could constitute a novel strategy in which tumour radiation sensitivity is improved secondary to metabolic remodelling rather than by altering intrinsic radiosensitivity.

AuNPs internalisation was concentration-dependent, displaying a clear positive correlation with treatment concentration under both normoxic and hypoxic conditions (Fig. 1). Of note, AuNP uptake under hypoxic conditions was at least comparable if not greater than that observed under aerobic conditions, indicating that hypoxic stress does not present a barrier to active AuNP internalisation. Indeed, emerging evidence suggests

that prolonged hypoxic exposure increases the retention of AuNPs within cells due to a reduction in intracellular vesicle trafficking and exocytosis (Neshatian et al. 2015). Differences in the NPs uptake are largely determined by specific cellular processes including endocytosis, exocytosis and autophagy (Chithrani et al. 2006; Gao et al. 2005; Chithrani and Chan 2007). When nanoparticles enter cells by receptor-mediated endocytosis, normally they remain constrained within endosomes prior to lysosomal fusion, degradation, and exocytosis. Prolonged hypoxic exposure results in a reduction in the supply of nutrients and energy, suppressing energy dependent processes such as autophagy and exocytosis (Shorer et al. 2005; Ma et al. 2011). Our results are consistent with findings which report that prolonged hypoxic exposure results in higher AuNP uptake in MCF-7 and HeLa cells, compared to equivalent normoxic conditions (Neshatian et al. 2015) Another plausible explanation is due to an increase in AuNP agglomeration under hypoxic conditions. Hypoxia, and in particular anaerobic metabolism is recognised as a common feature of most solid tumours, increasing extracellular lactic acid levels. This metabolic effect elevates the stromal pH of the tumour microenvironment, exposing AuNPs to environmental conditions that favour agglomeration (Neshatian et al. 2015; Sonveaux et al. 2008).

"Metabolic radiosensitisation" is conceptually based on altering the metabolic demand for oxygen consumption primarily by downregulating mitochondrial oxidative metabolism (Ashton et al. 2018). Increasing evidence suggests that decreasing oxygen consumption contributes to a reduction in hypoxia induced radioresistance (Ashton et al. 2016; Mey et al. 2018); Atovaquone targets and inhibits the function of mitochondrial complex III, as such we selected this anti-malarial drug to assess its ability to modulate radiation sensitivity. Our results demonstrate that atovaquone efficiently and rapidly (within two hours) suppresses OCR across all three cell lines, corroborating observations from existing reports in alternative tumour models (Kapur et al. 2022; Ashton et al. 2016) We also observed that atovaquone concomitantly triggered an increase in ECAR (Fig. 3d–f), indicating increased glycolytic function in response atovaquone mediated suppression of ATP production via oxidative phosphorylation. Such metabolic flexibility enables activation of various signalling pathways, compensating for loss of critical functions such as electron transport chain function, ultimately enabling survival under nutrient/oxygen deprivation. Additionally, the metabolic shift from oxidative metabolism to anaerobic glycolysis is recognised as contributing to undesirable effects with respect to the response to the radiotherapy, through elevated DNA damage repair and cancer stem cell enrichment (Bhatt et al. 2015; Li et al. 2016). Given the recognised role which glycolysis confers in mediating therapeutic resistance, glycolysis inhibitors could be used in combination with atovaquone to maximise the sensitising effect of these compounds in future studies.

AuNPs yielded significant positive radiation dose modifying effects in all three tumour cell models tested. Hypoxia is recognised as the main driver for the development of radioresistance via a series of mechanism, including impaired oxygen fixation at the time of radiation delivery, changes in cell cycle regulation, and/or the induction of anti-apoptotic genes (Boulefour et al. 2021). However, in our study, we found that hypoxic (0.5% O_2) cells were still sensitised to radiation by AuNPs. AuNP uptake is recognised as a key factor influencing radiosensitising potential. Zhang et al. (2008) highlighted the role of

surface functional groups on prostate cancer radiosensitivity comparing the uptake and radiosensitivity of thiol-glucose-capped AuNPs (Glu-AuNPs) and the neutral AuNPs (TGS-AuNPs), demonstrating that Glu-AuNPs resulted in a threefold increase in nanoparticle internalisation over TGS-AuNPs (Zhang et al. 2008). In keeping with the assertion that more intracellular gold results in greater radiosensitisation, Glu-AuNPs were more than twofold more effective when combined with radiotherapy compared with TGS-AuNPs. Our qualitative study using hyperspectral microscopy demonstrated that prolonged hypoxic exposure does not impair the nanoparticle uptake, nor differentially influence intracellular localisation (Fig. 1 and Additional file 1: Fig S1). Taken together, our quantitative and qualitative study of AuNPs uptake provide a solid rationale for AuNPs mediated radiosensitisation under hypoxic conditions.

The colony forming assay was used to establish both the direct impact of each individual component treatment on viability both ± radiation. Importantly, in the absence of radiation, neither AuNP treatment, atovaquone or combined AuNP/atovaquone treatment had any significant impact on colony formation, indicating that subsequent radiosensitisation effects are indeed a synergistic interaction as opposed to cumulative toxicity resulting from individual components (Additional file 1: Figure S3). Interestingly, treatment with atovaquone alone resulted in radiosensitisation in FaDu cells, leading to a significant increase in radiosensitivity (Fig. 4a), with greater effects observed when combined with AuNPs. More encouragingly, at the clinically relevant dose of 2 Gy, the combination of AuNPs and atovaquone significantly increased cell killing compared to radiation alone, producing a dose enhancement factor (DEF) of 1.5 over radiation alone (Additional file 1: Table S1). Similarly, the combination treatment also yielded the greatest effect under hypoxia (Additional file 1: Table S2), generating a mean DEF_{2Gy} of 1.25. In a clinical setting, dose enhancement on this scale could enable dose de-escalation helping to spare surrounding normal tissue from the adverse off-target effect of radiotherapy, or conversely if retaining an equivalent treatment plan markedly reduce the risk of treatment failure.

Next, we investigated the effect of combined AuNP and atovaquone treatment on cell cycle distribution, apoptosis and radiation-induced DNA damage repair. As outlined above, AuNP radiosensitisation is predominantly attributed to physical interactions between photons and high-Z material (Carter et al. 2007; Ghita et al. 2017) However, growing evidence suggests that AuNPs may also contribute to biological responses that arise following radiation interaction (Rosa et al. 2017) At present, four potential mechanisms contributing to the biological influence on AuNP radiosensitisation have been proposed including: cell cycle synchronisation, increased production of ROS and oxidative stress, DNA damage induction and an enhanced radiation bystander effect (Rosa et al. 2017); Roa et al. (2009) demonstrated AuNP mediated cell cycle acceleration through G_0/G_1 with an accumulation of cells in G_2/M via the activation of CDK kinase (Roa et al. 2009). The consequences of CDK activation were shown to deliver striking radiosensitisation, suggesting that cell cycle synchronisation played an important role in mediating such effect. Similarly, Geng et al. (2011) found that thiol-glucose coated AuNPs promoted G_2/M accumulation, contributing to an enhanced SKOV-3 cell sensitivity against MV X-ray radiation (Geng et al. 2011) The current study demonstrated that combined AuNPs and atovaquone treatment induced normoxic S-phase accumulation

(Fig. 5a). The sensitivity and subsequent biological impact of radiation is highly cell cycle dependent, with G_2/M recognised as the most sensitive phase to radiation (Pawlik and Keyomarsi 2004). Herein, the increase of S-phase cells appears to positively correlate with the radiosensitising effect, however, a mechanism for S-phase arrest remains unknown. Preliminary work suggests that functionality of the master tumour suppressor gene TP53 is believed to play a key role in mediating S-phase specific cell death (Ostruszka and Shewach 2000). All three cell lines used in the current study are TP53 mutant, therefore, these cells do not possess a competent G_1-S cell cycle checkpoint. As such, cell cycle progression is not stalled, limiting the opportunity for an increase in p21 to resolve or repair the damaged DNA. The ability to progress through cell cycle after radiation-induced damage is thought to synergistically enhance cell death, presenting a biological mechanism of radiosensitisation (Bélanger et al. 2014) As S-phase cells are considered more radioresistant than G_1-S or G_2-M cells, it can therefore be concluded that the radiosensitising effects caused by the combination of AuNPs and atovaquone are unlikely to be directly linked to the redistribution of cells to a more radiosensitive cell cycle phase (Pawlik and Keyomarsi 2004). Despite this, increased S-phase radiosensitivity is not unique to the current study. Kuno and Shinomiya (2000) demonstrated enhanced S-phase tumour killing activity following the treatment with the hypoxic radiosensitiser (PR-000350) (Kuno and Shinomiya 2000). Additionally, S-phase specific apoptosis is directly associated with a defect in nucleotide excision repair (NER), an important DNA damage repair process. Bélanger et al. (2014) reported that defective NER during S-phase increases apoptosis and reduces clonogenic survival in human melanoma cell lines following UV radiation treatment, an effect is mediated via the diminished activation of ataxia telangiectasia and Rad 3-related (ATR) kinase (Bélanger et al. 2014).

As S-phase specific death is linked to the activation of apoptosis, we also investigated the combined treatment effect of AuNPs and atovaquone on apoptotic fraction (Ray et al. 2007). Surprisingly, our work indicated that at the doses used atovaquone, AuNP or radiation alone did not significantly increase the apoptotic fraction, despite observing increased clonogenic radiosensitisation. This could likely be explained by delayed radiation cell death due to mitotic catastrophe. Firat et al. (2011) reported similar findings in a stem-like glioma cell (SLGCs) model that failed to trigger apoptosis four days after exposure to a single 10 Gy dose (Firat et al. 2011) However, four days post-radiation treatment 50% of the SLGCs tumours treated with 5 Gy or more observed delayed cell death. This effect was predominantly associated with cells lacking wild type TP53, attributing cell death to mitotic catastrophe. This finding highlights the important role of p53 in regulating the response to genotoxic damage. Interestingly, the combined effect of atovaquone, AuNP and radiation did significantly trigger the apoptosis in FaDu and CAL27 cells, within a comparatively short experimental timeframe. Gao et al. (2018) demonstrated that atovaquone significantly induced apoptosis in a concentration-dependent manner, inhibiting both cell proliferation and angiogenesis in vivo (Gao et al. 2018). Furthermore, Fu et al. (2020) reported that atovaquone triggers apoptosis in $EpCAM^{+}CD44^{+}$ tumour initiating HCT116 cells under hypoxia (Fu et al. 2020). Here we observed that AuNPs treatment alone is not enough to elicit strong apoptotic response, however, the apoptotic

fraction was increased following the combination treatment (Fig. 6a). This implies that stress caused by the inhibition of mitochondrial respiration by atovaquone may prime cells toward radiation-induced apoptosis.

Impaired DNA damage repair is another fundamental process that may contribute to the observed effects. Our data indicate that combined AuNPs and atovaquone results in more DNA damage at 2 and 24 h post treatment compared to cells treated with AuNP alone (Fig. 7 and Additional file 1: Fig S8). This effect is consistent with a previous report that 50 nm citrate capped AuNPs induce significant radiosensitisation in HeLa cells (Chithrani et al. 2010). To date, there are no direct studies evaluating DNA damage levels after atovaquone and radiation treatment. However, some reports suggests that atovaquone exhibits antitumour effects by increasing DNA damage. Ashton et al. (2016) reported that atovaquone increased radiosensitivity by inhibiting pyrimidine synthesis, thus negatively impacting both DNA damage repair and replication. Additionally, Gao et al. (2018) showed that atovaquone inhibits hepatoma cell proliferation by inducing double stranded DNA breaks, which contribute to the sustained ataxia -telangiectasia mutated (ATM) activation, and downstream molecules including cell cycle checkpoint kinase-2 (CHK2) and H2AX (Gao et al. 2018). In our work, we consistently observed a significant increase in the induction of lethal DNA double strand breaks (DSBs) after treatment with the combination of AuNP and atovaquone at both 2 h and 24 h (Fig. 7 and Additional file 1: Fig S8), an effect consistent with our clonogenic survival data. Interestingly, we observed that combination of atovaquone and AuNPs induce 47% increase in the yield of DSB induction for both initial (2 h) and residual damage (24 h) under hypoxia, indicating that the enhanced radiosensitivity from the combination of AuNPs and atovaquone may be due to the induction of greater DNA damage rather than negatively impacting the DNA damage repair process.

Conclusions

Overall, this work demonstrates the potential of combining AuNPs and atovaquone as a novel approach to enhance the radiotherapeutic effect in HPV(−) HNSCC. Treatment with atovaquone greatly reduced oxygen consumption in HNSCC cells, inducing a shift to a more glycolytic type, providing the basis for metabolic radiosensitisation. This approach appears to complement physical radiosensitisation conferred by AuNPs, inducing S-phase accumulation, contributing to greater DNA damage yields. Importantly, the combination results in superior radiotherapeutic effects compared to either agent alone. While this work provides a strong rationale for the combined use of physical and metabolic radiosensitisers, clinical translation will require careful consideration of critical parameters such as route of administration to avoid enhanced radiosensitivity of surrounding normal tissue. Given that external beam radiotherapy is delivered in a highly conformal manner, tumour specific radiosensitisation is by default achieved through accurate radiotherapy delivery. Furthermore, by adopting direct intra-tumoural injection as the means of delivery, the risk of off-target nanoparticle radiosensitisation can be further mitigated against. Indeed, this is the approach utilised by successful radiosensitising clinical studies using hafnium oxide nanoparticles, and in our opinion the option most likely to ultimately deliver clinical benefit from similar nanotechnologies.

Supplementary Information

The online version contains supplementary material available at https://doi.org/10.1186/s12645-023-00185-8.

Additional file 1: Table S1. Sensitiser enhancement ratio (SER) and dose enhancement factor (DEF) of HNSCC cells after treatment with AuNPs, atovaquone alone or the combination under normoxia (21% O_2). SER represents area under curve versus radiation only whilst DEF value demonstrates radiation enhancement at a single dose point versus radiation only. α and β component of linear quadratic has also been presented. **Table S2.** Sensitiser enhancement ratio (SER) and dose enhancement factor (DEF) of HNSCC cell after treatment with AuNPs, atovaquone alone or the combination under hypoxia (0.5% O_2). SER represents area under curve versus radiation only whilst DEF value demonstrates radiation enhancement at a single dose point versus radiation only. *α* and *β* component of linear quadratic has also been presented. **Figure S1.** Intracellular uptake and localisation of AuNPs within FaDu, CAL27 and CAL33 cells under hypoxia (0.5% O_2) using Cytoviva darkfield/hyperspectral imaging. Cells were treated with AuNPs for 24 h, fixed and mounted with DAPI before imaging. Representative images include enhanced dark field and the corresponding hyperspectral images, overlaid with a spectral angle map (SAM) representing AuNPs in red. **Figure S2.** Bioenergetic profile of HNSCC cells treated with atovaquone under hypoxic (0.5% O_2) conditions. Changes in oxygen consumption rate (OCR) and extracellular acidification rate (ECAR) were monitored at 37 °C for 3 h. The resulting effect of atovaquone on OCR and ECAR were shown as a percentage of the baseline measurement after each treatment. Data shown are the means ± SEM (*n*=5 per treatment group). **Figure S3.** SF_0 value of FaDu, CAL27 and CAL33 cells after treatment with AuNPs (100 µg) and/or atovaquone (AQ 30 µM) alone or in combination under both normoxia (21% O_2) and hypoxia (0.5% O_2). **Figure S4.** Flow cytometry analysis for cell cycle distribution of FaDu, CAL27 and CAL33 cells using propidium staining after treatment with AuNPs (100 µg) and/or atovaquone (AQ 30 µM) alone or in combination with radiation (4 Gy) under both normoxic (**a**) and hypoxic conditions (**b**). Experiments were performed in triplicate. **Figure S5.** Representative Annexin-V/-FITC/PI flow cytometry analysis of FaDu, CAL27 and CAL33 cells after treatment with AuNPs (100 µg) and/or atovaquone (AQ 30 µM) alone or in combination with radiation (4 Gy) under both normoxic (**a**) and hypoxic conditions (**b**). Experiments were performed in triplicate. **Figure S6.** A Representative immunofluorescence images of 53BP1 foci in CAL33 cells 24 h post radiation (2 Gy) under normoxia (21% O_2) and hypoxia (0.5% O_2). Cells were treated with either with AuNPs (100 µg), atovaquone (AQ, 30 µM) or the combination. Panels **b** and **c** represent mean 53BP1 foci 24 h post radiation (0 or 2 Gy) in CAL33 cells after treatment with AuNPs, atovaquone or the combination under normoxia (**b**) and hypoxia (**c**). Data presented are from at least three independent replicates performed in triplicates ± SEM. One way ANOVA followed by Turkey's multiple comparison test was used to compared within different treatment. * represents significant difference at $p<0.05$, ** at $p<0.01$, *** at $p<0.001$. **Figure S7.** A Representative immunofluorescence images of 53BP1 foci in CAL27 cells 24 h post radiation (2 Gy) under normoxia (21% O_2) and hypoxia (0.5% O_2). Cells were treated with either with AuNPs (100 µg), atovaquone (AQ, 30 µM) or the combination. Panel **b** and **c** represent mean 53BP1 foci 24 h post radiation (0 or 2 Gy) in CAL27 cells after treatment with AuNPs, atovaquone or the combination under normoxia (**b**) and hypoxia (**c**). Data presented are from at least three independent replicates performed in triplicates ± SEM. One way ANOVA followed by Turkey's multiple comparison test was used to compared within different treatment. *Represents significant difference at $p<0.05$. **Figure S8.** A Representative immunofluorescence images of 53BP1 foci in FaDu, CAL27 and CAL33 cells 2 h post radiation (2 Gy) under hypoxia (0.5% O_2). Cells were treated with either with AuNPs (100 µg), atovaquone (AQ, 30 µM) or the combination. Panel **b**, **c** and **d** represent mean 53BP1 foci 24 h post radiation (0 or 2 Gy) in FaDu (**b**), CAL27 (**c**) and CAL33 (**d**) cells after treatment with AuNPs, atovaquone or the combination under hypoxia. Data presented are from at least three independent replicates performed in triplicates ± SEM. One way ANOVA followed by Turkey's multiple comparison test was used to compared within different treatment. **Represents significant difference at $p<0.01$.

Acknowledgements
Not applicable

Author contributions
JF was the lead researcher conducting experimental work and in producing manuscript revisions. VP, NMB, TW, CY all made contributions to experimental design and execution. RM provided expertise and guidance on metabolic profiling in addition to reviewing and editing the manuscript. JC conceptualised work, assisted in experimental design, data interpretation and manuscript editing. All authors read and approved the final manuscript.

Funding
RJM is funded by the Dunhill Medical Trust RPFG1910/199, MRC MR/S036695/1, and the Department for the Economy Northern Ireland undertake US-Ireland R&D Partnership Programme with the Ref. USI 158.

Availability of data and materials
All data related to this study are present in the paper. Requests for access to raw data can be made through the corresponding author.

Declarations

Ethics approval and consent to participate
Not applicable.

Consent for publication
Not applicable.

Competing interests
The authors declare that they have no competing interests.

Received: 7 March 2023 Accepted: 29 March 2023
Published online: 08 April 2023

References

Araujo FG, Huskinson J, Remington JS (1991) Remarkable in vitro and in vivo activities of the hydroxynaphthoquinone 566C80 against tachyzoites and tissue cysts of *Toxoplasma* gondii. Antimicrob Agents Chemother 35(2):293–299
Ashton TM, Fokas E, Kunz-Schughart LA et al (2016) The anti-malarial atovaquone increases radiosensitivity by alleviating tumour hypoxia. Nat Commun 7:12308
Ashton TM, McKenna WG, Kunz-Schughart LA, Higgins GS (2018) Oxidative phosphorylation as an emerging target in cancer therapy. Clin Cancer Res 24(11):2482–2490
Bagley AF, Ludmir EB, Maitra A et al (2022) NBTXR3, a first-in-class radioenhancer for pancreatic ductal adenocarcinoma: report of first patient experience. Clin Transl Radiat Oncol 33:66–69
Bélanger F, Rajotte V, Drobetsky EA (2014) A Majority of human melanoma cell lines exhibits an s phase-specific defect in excision of uv-induced DNA photoproducts. PLoS ONE 9(1):e85294
Benej M, Hong X, Vibhute S et al (2018) Papaverine and its derivatives radiosensitize solid tumors by inhibiting mitochondrial metabolism. Proc Natl Acad Sci 115(42):10756–10761
Bennie LA, Feng J, Emmerson C et al (2021) Formulating RALA/Au nanocomplexes to enhance nanoparticle internalisation efficiency, sensitising prostate tumour models to radiation treatment. J Nanobiotechnology 19(1):1–13
Bentzen SM (2006) Preventing or reducing late side effects of radiation therapy: radiobiology meets molecular pathology. Nat Rev Cancer 6(9):702–713
Bhatt AN, Chauhan A, Khanna S et al (2015) Transient elevation of glycolysis confers radio-resistance by facilitating DNA repair in cells. BMC Cancer 15(1):1–12
Bittner M-I, Grosu A-L (2013) Hypoxia in head and neck tumors: characteristics and development during therapy. Front Oncol 3:223
Bol V, Bol A, Bouzin C et al (2015) Reprogramming of tumor metabolism by targeting mitochondria improves tumor response to irradiation. Acta Oncol (madr) 54(2):266–274
Bonner JA, Harari PM, Giralt J et al (2006) Radiotherapy plus cetuximab for squamous-cell carcinoma of the head and neck. N Engl J Med 354(6):567–578
Bonvalot S, Le Pechoux C, De Baere T et al (2017) First-in-human study testing a new radioenhancer using nanoparticles (NBTXR3) activated by radiation therapy in patients with locally advanced soft tissue sarcomas. Clin Cancer Res 23(4):908–917
Boulefour W, Rowinski E, Louati S et al (2021) A review of the role of hypoxia in radioresistance in cancer therapy. Med Sci Monit Int Med J Exp Clin Res 27:e934116–e934121
Bourigault P, Skwarski M, Macpherson RE, Higgins GS, McGowan DR (2021) Investigation of atovaquone-induced spatial changes in tumour hypoxia assessed by hypoxia PET/CT in non-small cell lung cancer patients. EJNMMI Res 11(1):1–10
Brizel DM, Sibley GS, Prosnitz LR, Scher RL, Dewhirst MW (1997) Tumor hypoxia adversely affects the prognosis of carcinoma of the head and neck. Int J Radiat Oncol Biol Phys 38(2):285–289
Brizel DM, Albers ME, Fisher SR et al (1998) Hyperfractionated irradiation with or without concurrent chemotherapy for locally advanced head and neck cancer. N Engl J Med 338(25):1798–1804
Butterworth KT, McMahon SJ, Currell FJ, Prise KM (2012) Physical basis and biological mechanisms of gold nanoparticle radiosensitization. Nanoscale 4(16):4830–4838
Carter JD, Cheng NN, Qu Y, Suarez GD, Guo T (2007) Nanoscale energy deposition by X-ray absorbing nanostructures. J Phys Chem B 111(40):11622–11625
Chen Y, Yang J, Fu S, Wu J (2020) Gold nanoparticles as radiosensitizers in cancer radiotherapy. Int J Nanomed 15:9407
Chithrani BD, Chan WCW (2007) Elucidating the mechanism of cellular uptake and removal of protein-coated gold nanoparticles of different sizes and shapes. Nano Lett 7(6):1542–1550
Chithrani BD, Ghazani AA, Chan WCW (2006) Determining the size and shape dependence of gold nanoparticle uptake into mammalian cells. Nano Lett 6(4):662–668
Chithrani DB, Jelveh S, Jalali F et al (2010) Gold nanoparticles as radiation sensitizers in cancer therapy. Radiat Res 173(6):719–728
Choi J, Kim G, Bin CS, Im H-J (2020) Radiosensitizing high-Z metal nanoparticles for enhanced radiotherapy of glioblastoma multiforme. J Nanobiotechnology 18(1):1–23
Cooper JS, Pajak TF, Forastiere AA et al (2004) Postoperative concurrent radiotherapy and chemotherapy for high-risk squamous-cell carcinoma of the head and neck. N Engl J Med 350(19):1937–1944
Cui L, Tse K, Zahedi P et al (2014) Hypoxia and cellular localization influence the radiosensitizing effect of gold nanoparticles (AuNPs) in breast cancer cells. Radiat Res 182(5):475–488
Cui L, Her S, Borst GR, Bristow RG, Jaffray DA, Allen C (2017) Radiosensitization by gold nanoparticles: Will they ever make it to the clinic? Radiother Oncol 124(3):344–356
Curtis KK, Wong WW, Ross HJ (2016) Past approaches and future directions for targeting tumor hypoxia in squamous cell carcinomas of the head and neck. Crit Rev Oncol Hematol 103:86–98
de Mey S, Jiang H, Corbet C et al (2018) Antidiabetic biguanides radiosensitize hypoxic colorectal cancer cells through a decrease in oxygen consumption. Front Pharmacol. https://doi.org/10.3389/fphar.2018.01073

Delaney G, Jacob S, Featherstone C, Barton M (2005) The role of radiotherapy in cancer treatment: estimating optimal utilization from a review of evidence-based clinical guidelines. Cancer Interdiscip Int J Am Cancer Soc 104(6):1129–1137
Dewey WC, Ling CC, Meyn RE (1995) Radiation-induced apoptosis: relevance to radiotherapy. Int J Radiat Oncol Biol Phys 33(4):781–796
Diepart C, Karroum O, Magat J et al (2012) arsenic trioxide treatment decreases the oxygen consumption rate of tumor cells and radiosensitizes solid tumors arsenic trioxide radiosensitizes solid tumors. Cancer Res 72(2):482–490
Eschmann S-M, Paulsen F, Reimold M et al (2005) Prognostic impact of hypoxia imaging with 18F-misonidazole PET in non-small cell lung cancer and head and neck cancer before radiotherapy. J Nucl Med 46(2):253–260
Fiorillo M, Lamb R, Tanowitz HB et al (2016) Repurposing atovaquone: targeting mitochondrial complex III and OXPHOS to eradicate cancer stem cells. Oncotarget 7(23):34084
Firat E, Gaedicke S, Tsurumi C, Esser N, Weyerbrock A, Niedermann G (2011) Delayed cell death associated with mitotic catastrophe in γ-irradiated stem-like glioma cells. Radiat Oncol 6(1):1–15
Fry M, Pudney M (1992) Site of action of the antimalarial hydroxynaphthoquinone, 2-[trans-4-(4′-chlorophenyl) cyclohexyl]-3-hydroxy-1, 4-naphthoquinone (566C80). Biochem Pharmacol 43(7):1545–1553
Fu C, Xiao X, Xu H, Lu W, Wang Y (2020) Efficacy of atovaquone on EpCAM+ CD44+ HCT-116 human colon cancer stem cells under hypoxia. Exp Ther Med 20(6):1
Gao H, Shi W, Freund LB (2005) Mechanics of receptor-mediated endocytosis. Proc Natl Acad Sci 102(27):9469–9474
Gao X, Liu X, Shan W et al (2018) Anti-malarial atovaquone exhibits anti-tumor effects by inducing DNA damage in hepatocellular carcinoma. Am J Cancer Res 8(9):1697
Geng F, Song K, Xing JZ et al (2011) Thio-glucose bound gold nanoparticles enhance radio-cytotoxic targeting of ovarian cancer. Nanotechnology 22(28):285101
Ghita M, McMahon SJ, Taggart LE, Butterworth KT, Schettino G, Prise KM (2017) A mechanistic study of gold nanoparticle radiosensitisation using targeted microbeam irradiation. Sci Rep 7(1):1–12
Gong L, Zhang Y, Liu C, Zhang M, Han S (2021) Application of radiosensitizers in cancer radiotherapy. Int J Nanomed 16:1083
Göttgens E-L, Ostheimer C, Span PN, Bussink J, Hammond EM (2018) HPV, hypoxia and radiation response in head and neck cancer. Br J Radiol 92(1093):20180047
Grimes DR, Kelly C, Bloch K, Partridge M (2014) A method for estimating the oxygen consumption rate in multicellular tumour spheroids. J R Soc Interface 11(92):20131124
Guo Y, Hu B, Fu B, Zhu H (2021) Atovaquone at clinically relevant concentration overcomes chemoresistance in ovarian cancer via inhibiting mitochondrial respiration. Pathol Pract 224:153529
Hainfeld JF, Slatkin DN, Smilowitz HM (2004) The use of gold nanoparticles to enhance radiotherapy in mice. Phys Med Biol 49(18):N309
Hainfeld JF, Dilmanian FA, Slatkin DN, Smilowitz HM (2008) Radiotherapy enhancement with gold nanoparticles. J Pharm Pharmacol 60(8):977–985
Her S, Jaffray DA, Allen C (2017) Gold nanoparticles for applications in cancer radiotherapy: mechanisms and recent advancements. Adv Drug Deliv Rev 109:84–101
Jain S, Coulter JA, Butterworth KT et al (2014) Gold nanoparticle cellular uptake, toxicity and radiosensitisation in hypoxic conditions. Radiother Oncol 110(2):342–347
Janic B, Brown SL, Neff R et al (2021) Therapeutic enhancement of radiation and immunomodulation by gold nanoparticles in triple negative breast cancer. Cancer Biol Ther 22(2):124–135
Jeremic B, Aguerri AR, Filipovic N (2013) Radiosensitization by gold nanoparticles. Clin Transl Oncol 15(8):593–601
Joiner MC, van der Kogel AJ (2018) Basic clinical radiobiology. CRC Press, Florida
Kapur A, Mehta P, Simmons AD et al (2022) Atovaquone: an inhibitor of oxidative phosphorylation as studied in gynecologic cancers. Cancers (basel) 14(9):2297
Kempson I (2021) Mechanisms of nanoparticle radiosensitization. Wiley Interdiscip Rev Nanomedicine Nanobiotechnology 13(1):e1656
Khoo AM, Cho SH, Reynoso FJ et al (2017) Radiosensitization of prostate cancers in vitro and in vivo to erbium-filtered orthovoltage X-rays using actively targeted gold nanoparticles. Sci Rep 7(1):1–13
Kuno Y, Shinomiya N (2000) PR-000350, a novel hypoxic radiosensitizer, enhances tumor cell killing by promoting apoptosis preferentially in the S-phase fraction. Apoptosis 5(1):69–77
Li X, Zhong Y, Lu J et al (2016) MtDNA depleted PC3 cells exhibit Warburg effect and cancer stem cell features. Oncotarget 7(26):40297
Linge A, Löck S, Gudziol V et al (2016) Low cancer stem cell marker expression and low hypoxia identify good prognosis subgroups in HPV (−) HNSCC after postoperative radiochemotherapy: a multicenter study of the DKTK-ROG. Clin Cancer Res 22(11):2639–2649
López-Valverde JA, Jiménez-Ortega E, Leal A (2022) Clinical feasibility study of gold nanoparticles as theragnostic agents for precision radiotherapy. Biomedicines 10(5):1214
Ma X, Wu Y, Jin S et al (2011) Gold nanoparticles induce autophagosome accumulation through size-dependent nanoparticle uptake and lysosome impairment. ACS Nano 5(11):8629–8639
Mirghani H, Amen F, Tao Y, Deutsch E, Levy A (2015) Increased radiosensitivity of HPV-positive head and neck cancers: molecular basis and therapeutic perspectives. Cancer Treat Rev 41(10):844–852
Neshatian M, Chung S, Yohan D, Yang C, Chithrani DB (2015) Uptake of gold nanoparticles in breathless (hypoxic) cancer cells. J Biomed Nanotechnol 11(7):1162–1172
Ostruszka LJ, Shewach DS (2000) The role of cell cycle progression in radiosensitization by 2′, 2′-difluoro-2′-deoxycytidine. Cancer Res 60(21):6080–6088
Pawlik TM, Keyomarsi K (2004) Role of cell cycle in mediating sensitivity to radiotherapy. Int J Radiat Oncol Biol Phys 59(4):928–942
Penninckx S, Heuskin A-C, Michiels C, Lucas S (2020) Gold nanoparticles as a potent radiosensitizer: a transdisciplinary approach from physics to patient. Cancers (basel) 12(8):2021

Perri F, Pacelli R, Della Vittoria Scarpati G et al (2015) Radioresistance in head and neck squamous cell carcinoma: biological bases and therapeutic implications. Head Neck 37(5):763–770
Ray S, Shyam S, Fraizer GC, Almasan A (2007) S-phase checkpoints regulate Apo2 ligand/TRAIL and CPT-11-induced apoptosis of prostate cancer cells. Mol Cancer Ther 6(4):1368–1378
Roa W, Zhang X, Guo L et al (2009) Gold nanoparticle sensitize radiotherapy of prostate cancer cells by regulation of the cell cycle. Nanotechnology 20(37):375101
Rockwell S, Dobrucki IT, Kim EY, Marrison ST, Vu VT (2009) Hypoxia and radiation therapy: past history, ongoing research, and future promise. Curr Mol Med 9(4):442–458
Rosa S, Connolly C, Schettino G, Butterworth KT, Prise KM (2017) Biological mechanisms of gold nanoparticle radiosensitization. Cancer Nanotechnol 8(1):2
Rupnow BA, Knox SJ (1999) The role of radiation-induced apoptosis as a determinant of tumor responses to radiation therapy. Apoptosis 4(2):115–143
Schuemann J, Bagley AF, Berbeco R et al (2020) Roadmap for metal nanoparticles in radiation therapy: current status, translational challenges, and future directions. Phys Med Biol 65(21):2102
Shaw R, Beasley N (2016) Aetiology and risk factors for head and neck cancer: United Kingdom National multidisciplinary guidelines. J Laryngol Otol 130(S2):S9–S12
Shorer H, Amar N, Meerson A, Elazar Z (2005) Modulation of N-ethylmaleimide-sensitive factor activity upon amino acid deprivation. J Biol Chem 280(16):16219–16226
Skwarski M, McGowan DR, Belcher E et al (2021) Mitochondrial inhibitor atovaquone increases tumor oxygenation and inhibits hypoxic gene expression in patients with non-small cell lung cancer atovaquone reduces tumor hypoxia in patients with NSCLC. Clin Cancer Res 27(9):2459–2469
Sonveaux P, Végran F, Schroeder T et al (2008) Targeting lactate-fueled respiration selectively kills hypoxic tumor cells in mice. J Clin Invest 118(12):3930–3942
Spiegelberg L, Houben R, Niemans R et al (2019) Hypoxia-activated prodrugs and (lack of) clinical progress: The need for hypoxia-based biomarker patient selection in phase III clinical trials. Clin Transl Radiat Oncol 15:62–69
Turkevich J, Stevenson PC, Hillier J (1951) A study of the nucleation and growth processes in the synthesis of colloidal gold. Discuss Faraday Soc 11:55–75
Verheij M, Bartelink H (2000) Radiation-induced apoptosis. Cell Tissue Res 301(1):133–142
Vermorken JB, Specenier P (2010) Optimal treatment for recurrent/metastatic head and neck cancer. Ann Oncol. https://doi.org/10.1093/annonc/mdq453
Wang H, Mu X, He H, Zhang X-D (2018) Cancer radiosensitizers. Trends Pharmacol Sci 39(1):24–48
Yasui H, Yamamoto K, Suzuki M et al (2017) Lipophilic triphenylphosphonium derivatives enhance radiation-induced cell killing via inhibition of mitochondrial energy metabolism in tumor cells. Cancer Lett 390:160–167
Zannella VE, Dal Pra A, Muaddi H et al (2013) Reprogramming metabolism with metformin improves tumor oxygenation and radiotherapy response. Clin Cancer Res 19(24):6741–6750
Zhang X, Xing JZ, Chen J et al (2008) Enhanced radiation sensitivity in prostate cancer by gold-nanoparticles. Clin Investig Med. https://doi.org/10.25011/cim.v31i3.3473

Publisher's Note